Nanosphere lithography: A materials general fabrication process for periodic particle array surfaces

John C. Hulteen and Richard P. Van Duyne[a)]
Department of Chemistry and Materials Research Center, Northwestern University, Evanston, Illinois 60208

(Received 17 October 1994; accepted 19 December 1994)

In this article nanosphere lithography (NSL) is demonstrated to be a materials general fabrication process for the production of periodic particle array (PPA) surfaces having nanometer scale features. A variety of PPA surfaces have been prepared using identical single-layer (SL) and double-layer (DL) NSL masks made by self-assembly of polymer nanospheres with diameter, $D=264$ nm, and varying both the substrate material S and the particle material M. In the examples shown here, S was an insulator, semiconductor, or metal and M was a metal, inorganic ionic insulator, or an organic π-electron semiconductor. PPA structural characterization and determination of nanoparticle metrics was accomplished with atomic force microscopy. This is the first demonstration of nanometer scale PPA surfaces formed from molecular materials. © *1995 American Vacuum Society.*

I. INTRODUCTION

Submicron device fabrication technologies based on optical lithography are reaching fundamental, diffraction limits as feature sizes approach 200 nm. The leading nanotechnologies for suboptical (viz., 10–200 nm) fabrication are electron-beam lithography (EBL)[1–4] and x-ray lithography (XRL).[4,5] Although EBL has outstanding resolution yielding features of 1–2 nm in the most favorable cases, its serial processing format is a limitation to achieving commercially acceptable throughputs of 1 cm^{-2} s^{-1}. XRL resolution is limited by photoelectron range and diffraction effects to 20–50 nm; however, its parallel processing capabilities that permit simultaneous fabrication of large numbers of nanostructures is an extremely advantageous feature.

Consequently there is substantial interest in developing nanofabrication techniques that combine the resolution of EBL with the throughput of XRL. Nanolithography based on the scanning tunneling microscope (STM) has received considerable attention[6] since it can image and manipulate matter on the atomic scale.[7,8] The application of STM lithography, like EBL, may be limited by serial processing speeds. Consequently novel approaches to parallel nanolithography are being explored including (1) diffusion-controlled aggregation at surfaces;[9] (2) laser-focused atom deposition;[10–12] and (3) nanometer-scale template formation from two-dimensional (2D) crystalline protein monolayers,[13] the pores of aluminum oxide thin films,[14] and self-assembled polymer nanospheres forming a single monolayer (SL), ordered mosaic array mask for deposition or reactive-ion etching.[15–20]

Deckman's "natural lithography" work attracted our attention because of its potential as an inexpensive, parallel, "bench-top" technique capable of fabricating Ag nanostructures for optical absorption studies related to surface-enhanced Raman spectroscopy (SERS),[21–23] quantum dot structures in GaAs-based semiconductors,[24–26] and high-T_c Josephson effect devices.[27] Our own work, which we refer to by the operationally more descriptive term of nanosphere lithography (NSL), has extended SL natural lithography in several ways:[28] (1) development of a double-layer (DL) polymer colloid mask; (2) atomic force microscopy (AFM) studies of SL and DL periodic particle arrays (PPAs) of Ag on mica; and (3) fabrication of defect-free SL and DL PPAs of Ag/mica with areas of 4–25 μm^2 that permit microprobe studies of nanoparticle optical properties.[29]

The experiments described in this article explore the versatility of NSL with respect to choice of substrate material S and deposition material M. A variety of PPA surfaces have been prepared using identical SL and DL NSL masks made with nanospheres of diameter, $D=264$ nm. In the examples shown below, S was chosen to be mica, Si(100), Si(111), or Cu(100) (viz., insulator, semiconductor, metal) and M was chosen to be Ag, CaF_2, and cobalt phthalocyanine (CoPc) (viz., metal, inorganic ionic insulator, organic π-electron semiconductor). AFM is used to characterize the nanostructure of the resultant PPA surfaces. This is believed to be the first demonstration of the formation of nanoscale PPAs based on molecular materials.

II. EXPERIMENT

A. Materials

Ag (99.99%, 0.50 mm diameter) and Au (99.99%, 0.50 mm diameter) were purchased from D. F. Goldsmith (Evanston, IL). Cr powder was purchased from Alpha Products, CaF_2 from Balzers and cobalt phthalocyanine from Kodak. Si(100) was purchased from Filmtronics, Inc. (Butler, PA), Si(111) from Silicon Quest International (Santa Clara, CA), glass microscope slides from American Scientific Products, and ruby red muscovite mica from Ashville-Schoonmaker Mica Co. (Newport News, VA). The Cu(100) surface was cut and polished using standard techniques from a single-crystal rod purchased from Materials Research Corporation (Orangeburg, NY). Tungsten vapor deposition boats were purchased from R. D. Mathis (Long Beach, CA).

[a)]Author to whom correspondence should be addressed; electronic mail: vanduyne@chem.nwu.edu

B. NSL mask preparation

The NSL masks were created by spin coating 264±7 nm polystyrene nanospheres, Interfacial Dynamics Corporation (Portland, OR), onto the substrate of interest at 3600 rpm on a custom-built spin coater. The physical dimensions of the substrate were chosen to be in the range 0.25–1.0 cm^2 and the entire substrate is spin coated with nanospheres. The nanospheres were received from the manufacturer as a suspension in water, and then further diluted in a solution of the surfactant Triton X-100/methanol (1:400 by volume) before spin coating. The surfactant was used to assist the solutions in wetting the substrate. Double-layer masks were created by increasing the nanosphere concentration in the spin coating solution as compared to the single-layer mask concentration. The specimen-to-specimen reproducibility of NSL mask preparation is excellent. For the $D=264$ nm nanospheres used in this article, 90% of the specimens were successfully coated with large domains of defect-free packing over the entire substrate surface.

C. Deposition of M

Thin films of M were deposited in a modified Consolidated Vacuum Corporation vapor deposition system with a base pressure of 10^{-7} Torr. The mass thickness d_m and deposition rate r_d were measured for each film with a custom-built quartz-crystal microbalance that was calibrated by both cyclic voltametry and STM.[30] Samples were mounted 240 mm above the effusive source with three 25-mm-diam apertures regularly spaced between the source and the sample which provided collimation or the PVD beam.

D. Nanosphere liftoff

After deposition of M=Ag, Au, Cr, or CaF_2, the polystyrene nanospheres were removed from S by dissolving them in CH_2Cl_2 with the aid of sonication for 1–4 min. For those experiments involving M=CoPc, the nanospheres were removed mechanically by transparent tape liftoff since sonication in CH_2Cl_2 also dissolved the CoPc nanoparticles. Although the tape liftoff does not remove all the nanospheres, large area AFM images show that sphere-free domains >100 μm^2 can be easily fabricated by this procedure.

E. AFM measurements

All AFM images were collected either in air or under an $N_2(g)$ environment on a Digital Instruments Nanoscope II microscope. Etched Si nanoprobe tips, Digital Instruments, with spring constants of approximately 0.15 $N\,m^{-1}$ were used. These tips are conical in shape with a cone angle of 20° and an effective radius of curvature at the tip, $R_c=10$ nm. The sharp features of these tips were necessary to reduce tip-induced image broadening and to decrease the effect of capillary forces with the surface. The images reported here are raw, unfiltered data collected in the constant force mode with the applied force between 3 and 30 nN [under $N_2(g)$ versus in air) and a scan speed of 8 lines s^{-1}. The scan head had a range of 12 μm×12 μm.

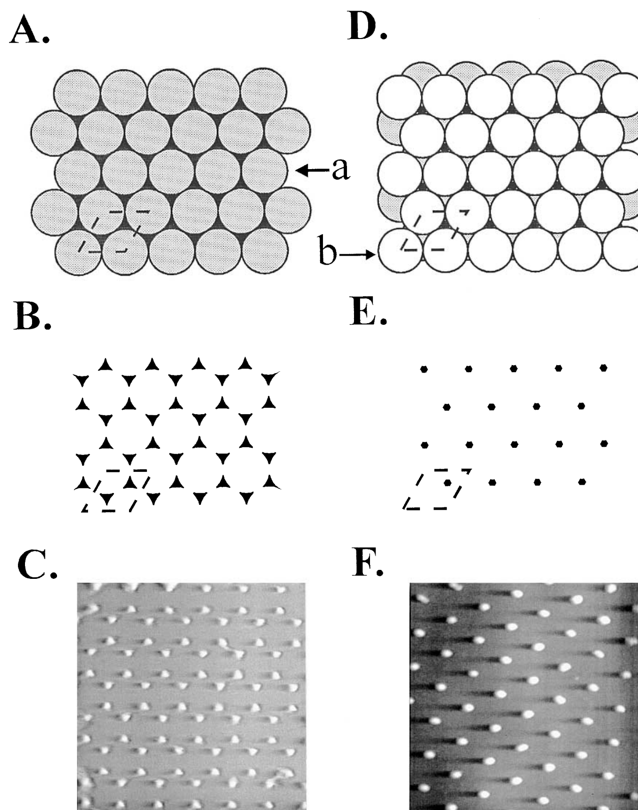

FIG. 1. Schematic diagrams of single-layer (SL) and double-layer (DL) nanosphere masks and the corresponding periodic particle array (PPA) surfaces. (A) $a(111)$ SL mask, dotted line=unit cell, a=first layer nanosphere; (B) SL PPA, 2 particles per unit cell; (C) 1.7×1.7 μm constant height AFM image of a SL PPA with M=Ag, S=mica, $D=264$ nm, $d_m=22$ nm, $r_d=0.2$ nm s^{-1}. (D) $a(111)p(1\times1)$-b DL mask, dotted line=unit cell, b=second layer nanosphere; (E) DL PPA, 1 particle per unit cell; (F) 2.0 ×2.0 μm constant height AFM image of a DL PPA with M=Ag, S=mica, $D=264$ nm, $d_m=22$ nm, $r_d=0.2$ nm s^{-1}.

III. RESULTS AND DISCUSSION

A. NSL mask characteristics

Figure 1 schematically illustrates the nanosphere lithography process for creating PPA surfaces from both SL and DL masks. The first step [Fig. 1(A)] in fabricating a SL PPA surface involves spin coating a single monolayer of nanospheres with chosen diameter D on substrate S. The surface symmetry of the SL mask is $a(111)$ where a represents a first-layer nanosphere. In the second step, a thin film of deposition material M is deposited to a mass thickness d_m over the nanosphere-coated substrate. The third step is nanosphere liftoff by chemical or mechanical means. Deposition material that penetrates the threefold holes of the SL mask remains on the substrate forming the SL PPA pattern [Fig. 1(B)]. The particle metrics of these PPA surfaces are defined from the mask geometry. The interparticle spacing $d_{\mathrm{ip,SL}}^{\mathrm{geom}}$ for the SL PPA is given by

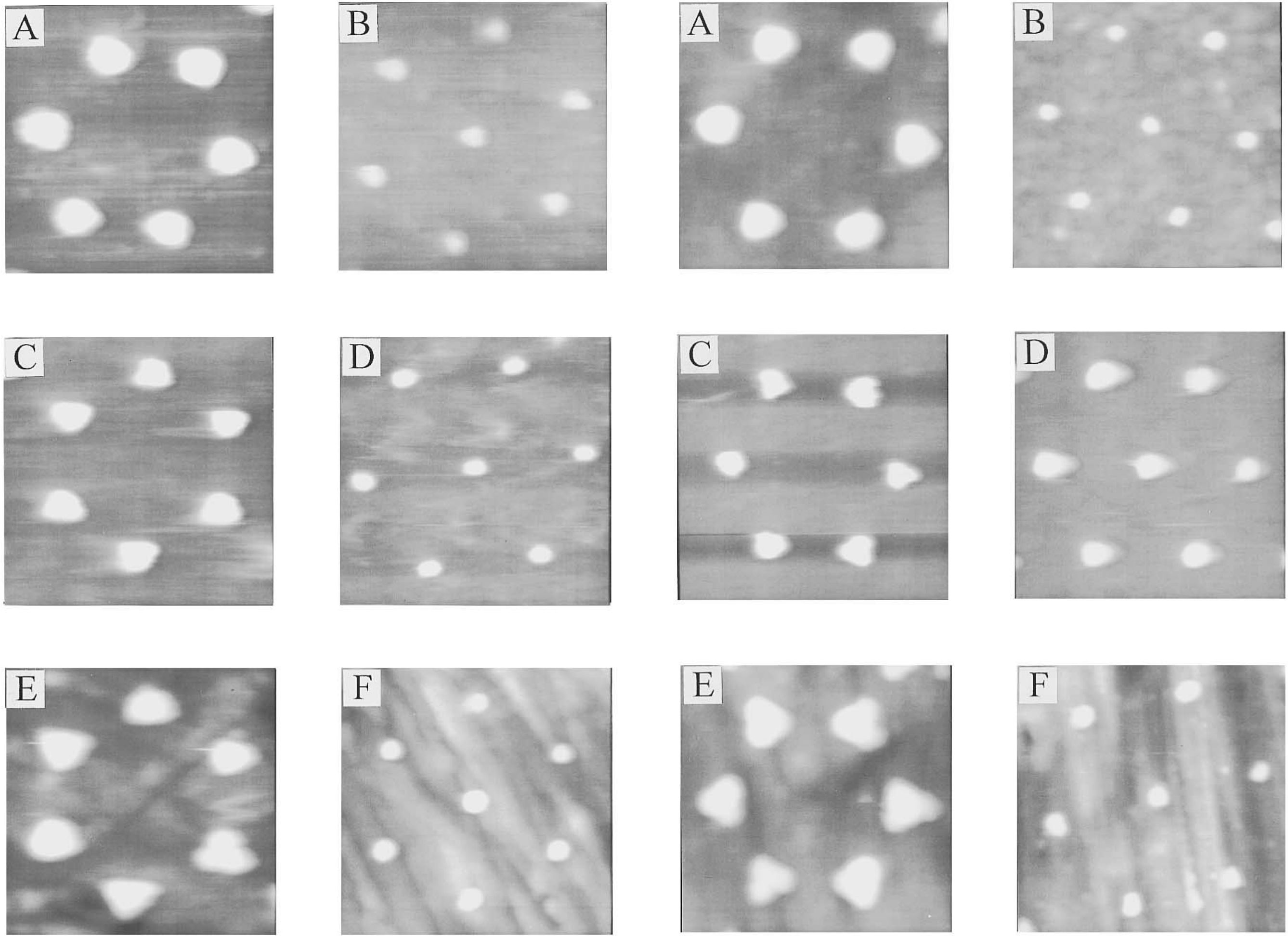

FIG. 2. AFM images of SL and DL PPAs of M=Ag on S=mica, Si(100), and Au(poly). (A) Ag SL PPA on mica, 420×420 nm image. (B) Ag DL PPA on mica, 740×740 nm image. (C) Ag SL PPA on Si(100), 470×470 nm image. (D) Ag DL PPA on Si(100), 676×676 nm image. (E) Ag SL PPA on polycrystalline Au, 415×415 nm image. (F) Ag DL PPA on polycrystalline Au, 787×787 nm image.

FIG. 3. AFM images of SL and DL PPAs of M=Ag on S=glass, Si(111), and Cu(100). (A) Ag SL PPA on glass, 437×437 nm image. (B) Ag DL PPA on glass, 757×757 nm image. (C) Ag SL PPA on Si(111), 515×515 nm image. (D) DL PPA on Si(111), 805×805 nm image. (E) Ag SL PPA on Cu(100), 490×490 nm image. (F) Ag DL PPA on Cu(100), 738×738 nm image.

$$d_{\mathrm{ip,SL}}^{\mathrm{geom}}=\frac{D}{\sqrt{3}}=0.577D \tag{1}$$

and the in-plane particle diameter $a_{\mathrm{SL}}^{\mathrm{geom}}$ defined as the perpendicular bisector of the largest inscribed equilateral triangle that fills the threefold hole, is given by

$$a_{\mathrm{SL}}^{\mathrm{geom}}=\frac{3}{2}\left(\sqrt{3}-1-\frac{1}{\sqrt{3}}\right)D=0.233D. \tag{2}$$

The out-of-plane particle height b_{SL} is not governed by the properties of the NSL mask, but should be equal to d_m of the deposited film of material M. The AFM image shown in Fig. 1(C) illustrates that NSL is capable of fabricating SL PPAs of Ag/mica with defect-free areas sufficiently large (viz., ~4 $\mu\mathrm{m}^2$) to probe the optical properties of Ag nanoparticles with far-field, diffraction limited focus, spatially resolved SERS (SR-SERS), and related techniques.[29–32]

A DL NSL mask is generated by spin coating with a higher concentration suspension of nanospheres. In such circumstances a second layer of nanospheres is deposited to form a mask that possesses $a(111)p(1\times1)\text{-}b$ surface symmetry [Fig. 1(D)]. Here a represents a nanosphere in the first layer and b represents a nanosphere in the second layer. Deposition of M over the DL mask to a thickness d_m results in penetration of every other threefold hole in the first layer of nanospheres since there is a corresponding blocking nanosphere in the second layer for half the threefold holes. Nanospheres liftoff results in the pattern of nanoparticles schematically shown in Fig. 1(E) and the AFM image shown in Fig. 1(F) illustrates the realization of this pattern over a 4 $\mu\mathrm{m}^2$ defect-free area. Each particle should be hexagonal in shape and from the geometry of the mask we find that $d_{\mathrm{ip,DL}}^{\mathrm{geom}}$ is given by

$$d_{\mathrm{ip,DL}}^{\mathrm{geom}}=D, \tag{3}$$

$a_{\mathrm{DL}}^{\mathrm{geom}}$ is given by

$$a_{\mathrm{DL}}^{\mathrm{geom}}=\left(\sqrt{3}-1-\frac{1}{\sqrt{3}}\right)D=0.155D \tag{4}$$

TABLE I. Experimental particle characteristics for PPAs formed from M=Ag on various S.

	SL PPAs					DL PPAs				
S	$d_{\mathrm{ip,SL}}$ (nm)	a_{SL}[a] (nm)	b_{SL} (nm)	d_m (nm)	r_d (nm s^{-1})	$d_{\mathrm{ip,DL}}$ (nm)	a_{DL}[a] (nm)	b_{DL} (nm)	d_m (nm)	r_d (nm s^{-1})
Mica	152±5	50±3	23±1	22	0.2	267±7	45±4	23±1	22	0.2
Si(100)	152±5	36±2	23±1	22	0.2	267±7	32±2	18±1	22	0.2
Au(poly)	152±5	57±4	22±2	22	0.2	267±7	45±3	20±1	22	0.2
Glass	152±5	46±3	20±1	22	0.2	267±7	35±2	21±1	22	0.2
Si(111)	152±5	43±4	17±1	18	0.2	267±7	64±3[b]	16±1	18	0.2
Cu(100)	152±5	66±2	20±2	22	0.2	267±7	44±2	18±1	22	0.2

[a]Corrected for tip broadening assuming rectangular out-of-plane particle cross section.
[b]a_{DL} should be $<a_{\mathrm{SL}}$. This anomaly is due to imaging with a damaged tip with large R_c.

and $b_{\mathrm{DL}}=d_m$. In a recent study of SL and DL PPAs by quantitative AFM imaging, it was shown that the standard deviation of d_{ip} and a for the materials system S=mica and M=Ag was dictated entirely by the standard deviation σ_D of the nanosphere diameter distribution.[28] Most nanospheres can be purchased with $\sigma_D \leqslant 0.04D$ and d_m is typically reproducible to ± 1 nm, so rather narrow d_{ip}, a, and b histograms can be found for nanoparticles fabricated by NSL.

B. NSL on insulator, semiconductor, and metal substrates

The capability of NSL to pattern a variety of substrates with a single-deposition material using both SL and DL masks self-assembled from $D=264$ nm nanospheres is presented in Figs. 2 and 3. These figures show AFM micrographs of NSL generated PPAs in which M=Ag was deposited over S=mica, Si(100), polycrystalline Au, glass, Si(111), and Cu(100) to a thickness d_m=18–22 nm. These results clearly show the ability of NSL to form SL and DL PPA patterns of a metal on insulator, semiconductor, and metal substrates.

An important question to address is—How accurately is the same SL and DL mask pattern reproduced for the same M on different S? Table I lists AFM measurements of the SL and DL PPA nanoparticle metrics for the six substrate surfaces studied. Each measurement represents the average from 10 to 20 particles collected near the field of the AFM images shown in Figs. 2 and 3. The experimental data for $d_{\mathrm{ip,SL}}$, a_{SL}, $d_{\mathrm{ip,DL}}$, and a_{DL} in Table I should be compared with the geometric predictions of Eqs. (1)–(4) and b_{SL} and b_{DL} should be compared with d_m. For $D=264\pm 8$ nm the geometrically defined metrics are $d_{\mathrm{ip,SL}}^{\mathrm{geom}} = 152\pm 8$ nm, $a_{\mathrm{SL}}^{\mathrm{geom}}=62\pm 8$ nm, $d_{\mathrm{ip,DL}}^{\mathrm{geom}}=264\pm 8$ nm, and $a_{\mathrm{DL}}^{\mathrm{geom}}=41\pm 8$ nm. The values of $d_{\mathrm{ip,SL}}^{\mathrm{expt}}=152\pm 5$ nm and $d_{\mathrm{ip,DL}}^{\mathrm{expt}}=267$

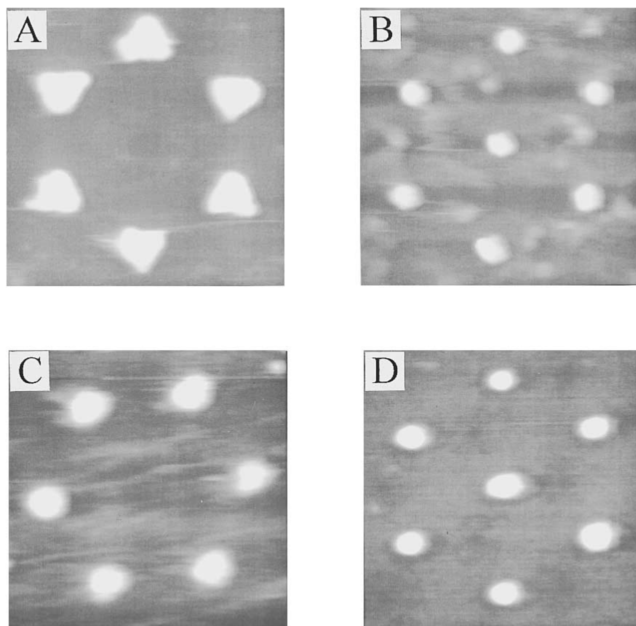

FIG. 4. AFM images of SL and DL PPAs of M=Au and Cr on S=Si(100). (A) Au SL PPA on Si(100), 473×473 nm image. (B) Au DL PPA on Si(100), 780×780 nm image. (C) Cr SL PPA on Si(100), 444×444 nm image. (D) Cr DL PPA on Si(100), 762×762 nm image.

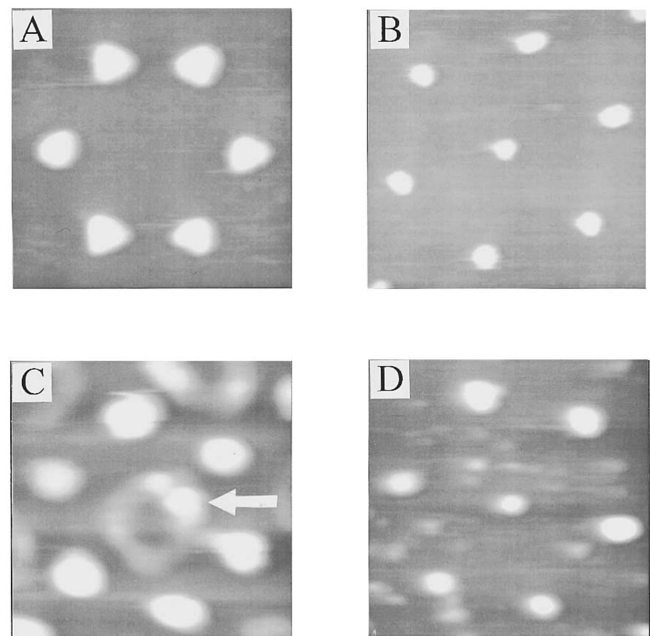

FIG. 5. AFM images of SL and DL PPAs of M=CaF_2 and CoPc on Si(100). (A) CaF_2 SL PPA on Si(100), 513×513 nm image. (B) CaF_2 DL PPA on Si(100), 748×748 nm image. (C) CoPc SL PPA on Si(100), 465×465 nm image. The object in the center of image (c) (shown by an arrow) is a small section of a polystyrene nanosphere remaining on the surface after mechanical nanosphere liftoff. (D) CoPc DL PPA on Si(100), 728×728 nm image.

TABLE II. Experimental particle characteristics for PPAs formed from various M on S=Si(100).

	SL PPAs					DL PPAs				
M	$d_{ip,SL}$ (nm)	a_{SL} (nm)	b_{SL} (nm)	d_m (nm)	r_d (nm s^{-1})	$d_{ip,DL}$ (nm)	a_{DL} (nm)	b_{DL} (nm)	d_m (nm)	r_d (nm s^{-1})
Ag	152±5	36±2[a]	23±1	22	0.2	267±7	32±2[a]	18±1	22	0.2
Au	152±5	53±3[a]	19±1	20	0.1	267±7	51±3[a]	16±1	20	0.1
Cr	152±5	62±3[b]	8±1	10	0.05	267±7	48±3[a]	17±1	15	0.05
CaF_2	152±5	55±5[a]	19±1	20	0.1	267±7	43±3[a]	18±1	20	0.1
CoPc	152±5	49±5[a]	18±3	20	0.5	267±7	65±8[b,c]	9±1	20	0.5

[a]Corrected for tip broadening assuming rectangular out-of-plane particle cross section.
[b]Corrected for tip broadening assuming trapezoidal out-of-plane particle cross section.
[c]a_{DL} should be $<a_{SL}$. This anomaly may be due to an angle of deposition not equal to 0° in this experiment.

± 7 nm (Table I) are in excellent agreement with those predicted. Likewise, b_{SL} and b_{DL} (Table I) show no systematic deviations from the expected value of d_m. In contrast the experimental values of a_{SL}^{expt} and a_{DL}^{expt} (Table I), which were corrected to remove tip-induced particle broadening,[28] show significant deviations from the geometric predictions except for the Ag/Cu(100) system which is in excellent agreement. For the other nanoparticle systems we find that (1) the values of a_{SL}^{expt} and a_{DL}^{expt} (Table I) *corrected for tip broadening* are always *smaller* than $a_{SL}^{geom}$and $a_{DL}^{geom}$with the exception of a_{DL}^{expt} for Ag/Si(111) which we have traced to imaging with a damaged tip having a large R_c and (2) the deviations for a_{SL}^{expt} are systematically larger than for a_{DL}^{expt}. This disparity between a^{geom} and a^{expt} is likely to have its origin in at least two effects. These are illustrated using the example of SL nanoparticles. First, the value of a_{SL}^{geom} was based on the assumption that the shape of an SL nanoparticle was adequately represented as an equilateral triangle. Examination of Figs. 2(A), 2(C), 2(E), 3(A), 3(C), and 3(E) shows triangular-shaped nanoparticles for the Ag/Cu(100) and possibly the Ag/Au(poly) systems and shows distinctly rounded shapes for the other SL nanoparticle systems. This difference between the assumed and the actual nanoparticle shapes would lead to $a_{SL}^{expt} < a_{SL}^{geom}$. Second, the correction applied to the raw a_{SL}^{expt} data for the effects of tip-induced broadening was based on the assumption that SL nanoparticles had rectangular out-of-plane cross sections. If the actual sample of SL nanoparticles has rounded (e.g., hemi-ellipsoidal) cross sections, applying a correction based on the assumption of a rectangular cross-section nanoparticle would also lead to $a_{SL}^{expt} < a_{SL}^{geom}$. Further studies measuring a_{SL}^{expt} and a_{DL}^{expt} as a function of d_m are needed to experimentally determine what geometric model of the out-of-plane cross section best represents the data.

C. NSL of metal and molecular deposition materials on Si(100)

The capability of NSL to pattern a single substrate with various deposition materials using both SL and DL masks self-assembled from $D=264$ nm nanospheres is presented in Figs. 4 and 5. These figures show AFM micrographs of NSL generated PPAs in which deposition materials M=Ag, Au, Cr, CaF_2, and CoPc are deposited over S=Si(100) to a thickness, d_m=10–20 nm. These results clearly show the ability of NSL to form SL and DL PPA patterns of metals, an inorganic ionic solid insulator, and an organic molecular π-electron semiconductor on a semiconductor substrate.

The accuracy of SL and DL PPA patterns for different M on the same S is addressed in Table II which lists AFM measurements of the nanoparticle metrics. The data in Table II were collected in a manner identical to that in Table I. Likewise, comparison of the data in Table II with the geometric results of Eqs. (1)–(4) and d_m is also similar. The values of $d_{ip,SL}^{expt}=152\pm5$ nm and $d_{ip,DL}^{expt}=267\pm7$ nm (Table II) agree within experimental error with $d_{ip,SL}^{geom}$ and $d_{ip,DL}^{geom}$. With the exception of b_{DL} for M=CoPc, b_{SL} and b_{DL} agree with d_m for all M/Si(100) systems. The $b_{DL}<d_m$ anomaly for CoPc/Si(100) has been traced to a deposition run in which the CoPc effusive beam was not perpendicular to the NSL mask. The tip-broadening corrected values of a_{SL}^{expt} and a_{DL}^{expt} (Table II) for several M/Si(100) systems show significant deviations from the geometric predictions. At the extremes, the deviations are 26 nm low for SL M=Ag and 24 nm high for DL M=CoPc. In contrast, the Cr/Si(100) and CaF_2/Si(100) systems exhibit both a_{SL}^{expt} and a_{DL}^{expt} within a few nanometers of expectations. Sufficient systematic studies have not yet been performed to determine the origin of these deviations; however, we anticipate that for the most part they are due to deviations from the in-plane triangular and out-of-plane rectangular particle shapes assumed in the data analysis.

IV. CONCLUSIONS

Nanosphere lithography has been demonstrated to be a simple, bench-top, materials general approach to high quality PPA nanostructures. NSL provides excellent control of interparticle spacing and out-of-plane height to the level of a few nanometers. Control of in-plane particle diameter, in-plane particle shape, and out-of-plane particle cross section is adequate for some fundamental studies, but will need improvement for device applications. One of the most intriguing results of this work is that inorganic and organic molecular materials can be processed by NSL into PPAs. To our knowledge this is the first demonstration of PPAs with molecule-based materials. PPA nanostructures can now be envisioned for applications such as fundamental studies of material

properties as a function of particle size, quantum dot arrays, single-electron transistors, and the electrochemistry of nanometer-sized structures.

ACKNOWLEDGMENTS

This work was supported by the National Science Foundation (CHE-940078) and by the Northwestern University Materials Research Center (DMR-9120521).

[1]H. G. Craighead and P. M. Mankiewich, J. Appl. Phys. **53**, 7186 (1982).
[2]H. G. Craighead, in *Microbeam Analysis*, edited by A. G. Romig, Jr. and J. I. Goldstein (San Francisco Press, San Francisco, 1984), p. 73.
[3]R. F. Pease, in *Nanostructures and Mesoscopic Systems*, edited by W. P. Kirk and M. A. Reed (Academic, Boston, 1992), p. 37.
[4]R. F. W. Pease, J. Vac. Sci. Technol. B **10**, 278 (1992).
[5]H. I. Smith and M. L. Schattenburg, IBM J. Res. Dev. **37**, 319 (1993).
[6]J. A. Dagata and C. R. K. Marrian, *Technology of Proximal Probe Lithography* (SPIE, Bellingham, WA, 1993), Vol. 10.
[7]D. M. Eigler and E. K. Schweizer, Nature **344**, 524 (1990).
[8]J. A. Stroscio and D. M. Eigler, Science **254**, 1319 (1991).
[9]H. Röder, E. Hahn, H. Brune, J.-P. Bucher, and K. Kern, Nature **366**, 141 (1993).
[10]G. Timp, R. E. Behringer, D. M. Tennant, J. E. Cunningham, M. Pretiss, and K. K. Berggren, Phys. Rev. Lett. **69**, 1636 (1992).
[11]J. J. McClelland, R. E. Scholten, E. C. Palm, and R. J. Celotta, Science **262**, 877 (1993).
[12]R. E. Scholten, J. J. McClelland, E. C. Palm, A. Gavrin, and R. J. Celotta, J. Vac. Sci. Technol. B **12**, 1847 (1994).
[13]K. Douglas, G. Devaud, and N. A. Clark, Science **257**, 642 (1992).
[14]C. A. Foss, Jr., G. L. Hornyak, J. A. Stockert, and C. R. Martin, J. Phys. Chem. **98**, 2963 (1994).
[15]H. W. Deckman and J. H. Dunsmuir, Appl. Phys. Lett. **41**, 377 (1982).
[16]H. W. Deckman and J. H. Dunsmuir, J. Vac. Sci. Technol. B **1**, 1109 (1983).
[17]C. B. Roxlo, H. W. Deckman, and B. Ables, Phys. Rev. Lett. **57**, 2462 (1986).
[18]H. W. Deckman and J. H. Dunsmuir, U.S. Patent No. 4,407,695 (1987).
[19]H. W. Deckman and T. D. Moustakas, J. Vac. Sci. Technol. B **6**, 316 (1988).
[20]H. W. Deckman, J. H. Dunsmuir, S. Garoff, J. A. McHenry, and D. G. Peiffer, J. Vac. Sci. Technol. B **6**, 333 (1988).
[21]B. K. Russell, J. G. Mantovani, V. E. Anderson, R. J. Warmack, and T. L. Ferrell, Phys. Rev. B **35**, 2151 (1987).
[22]M. C. Buncick, R. J. Warmack, and T. L. Ferrell, J. Opt. Soc. Am. B **4**, 927 (1987).
[23]E. A. Wachter, A. Moore, and J. W. Haas III, Vib. Spectrosc. **3**, 73 (1992).
[24]H. Fang, R. Zeller, and P. J. Stiles, Appl. Phys. Lett. **55**, 1433 (1989).
[25]T. Iwabuchi, C. Chuang, G. Khitrova, M. E. Warren, A. Chavez-Pirson, H. M. Gibbs, D. Sarid, and M. Gallagher, Proc. SPIE **1284**, 142 (1990).
[26]M. Green, M. Garcia-Parajo, and F. Khaleque, Appl. Phys. Lett. **62**, 264 (1993).
[27]W. D. Dozier, K. P. Daly, R. Hu, C. E. Platt, and M. S. Wire, IEEE Trans. Magn. **MAG-27**, 3223 (1990).
[28]R. P. Van Duyne, J. C. Hulteen, and D. A. Treichel, Science (to be published).
[29]D. A. Treichel, Ph.D. dissertation, Northwestern University, Evanston, IL, 1993.
[30]R. P. Van Duyne, J. C. Hulteen, and D. A. Treichel, J. Chem. Phys. **99**, 2101 (1993).
[31]R. P. Van Duyne, K. L. Haller, and R. I. Altkorn, Chem. Phys. Lett. **126**, 190 (1986).
[32]K. L. Haller, L. A. Bumm, R. A. Altkorn, E. J. Zeman, G. C. Schatz, and R. P. Van Duyne, J. Chem. Phys. **90**, 1237 (1989).